



**Asymmetric photoelectron momentum distribution of carbon monoxide**H. B. Ambalampitiya  and J. M. Ngoko Djiokap *Department of Physics and Astronomy, University of Nebraska, Lincoln, Nebraska 68588-0299, USA*

(Received 30 November 2023; revised 23 February 2024; accepted 19 March 2024; published 8 April 2024)

The photoelectron momentum distribution (PMD) for the linear (in intensity) process of one-photon single ionization of carbon monoxide is examined in the polarization plane for several orientations of the linear polarization vector with respect to the molecular axis. For a pulse bandwidth broader than the energy gap between the highest occupied molecular orbital (HOMO) and HOMO-1, the PMD is found to be mixed with HOMO and HOMO-1 signatures because electrons are emitted from these initial orbitals. We show that the asymmetry of the HOMO is strongly revealed in the PMD for any molecular orientation. The backward-forward asymmetry in the PMD and the normalized asymmetry are used as probes of the degree of mixing.

DOI: [10.1103/PhysRevA.109.043108](https://doi.org/10.1103/PhysRevA.109.043108)**I. INTRODUCTION**

A main goal of attosecond science is controlling electronic motion in matter on its natural attosecond timescale, which implies liberating electrons from atoms and molecules (the building block of matter) with high asymmetry [1]. Although the investigations and control of ultrafast electron dynamics in molecules have huge potential to understand a large variety of chemical processes [2], most proposals that employ a single extreme ultraviolet (XUV) laser pulse in realizing asymmetric angular distributions of electrons rely on interference phenomena in atoms [3–11]. The strategy there consists of using the laser pulse's broad bandwidth—characteristic of a few-cycle XUV isolated attosecond pulse [12–18]—to create broad electron energy distributions for the nonlinear process of above-threshold ionization (ATI) discovered in 1979 by Pierre Agostini *et al.* [19], with strong interference happening between successive ATI peaks. Since the final states of the photoelectrons created between ATI peaks have opposite parity, such interferences lead inevitably to the so-called forward-backward asymmetry in the angular distribution of the photoelectron, controllable by the pulse carrier-envelope phase (CEP) [3–11], or adjustable by electron-electron correlation in correlated processes [9–11].

Due to the nonlinearity nature of these atomic processes by a single laser pulse combined with major technological challenges in producing *intense enough* ultrashort light source *with stabilized CEP in the XUV regime*, the experimental demonstration of the forecasted forward-backward asymmetry effect produced by a single laser XUV pulse is not yet a reality. While strides in improving the imperfections of the pulses from high-order harmonic generation (HHG) [16–18, 20–23] or free-electron laser (FEL) [24–28] are being made, anisotropy in the photoelectron angular distribution has been demonstrated by coherent control using more than one laser pulse [29–31]. In contrast to those previous works [29–31], here for a single XUV laser pulse we show in this contribution that switching the atomic targets to linear molecular ones but with large permanent electric dipole moment appears to be a suitable way to mitigate the

nonlinearity problem by relaxing the constraints imposed on the laser pulse properties in order to liberate electrons with high asymmetry in a controllable and efficient manner from a linear uncorrelated process, not a nonlinear and correlated one.

It is well known in quantum chemistry that when two atoms with large contrast in their electronegativities bond together, the orbital energies of the most electronegative atom downshift and the resulting molecular orbital possesses large permanent electric dipole moment, e.g., in HF, NO, and CO. In contrast to atoms, the origin of the backward-forward asymmetry reported here and also discussed in Refs. [32–34] in a heteronuclear diatomic molecule resides in the intrinsic asymmetry property of the initial ionizing orbital, which turns out to be directly mapped out in the momentum distribution of the continuum electron created by one-photon absorption transition.

The anisotropy in the photoelectron momentum distribution (PMD) of CO (a closed-shell molecule) has been studied in the context of stereo Wigner time delay (SWTD) using the streaking technique [32] or the RABBITT technique [33]. A recent study [34] on asymmetric PMD in NO (an open-shell molecule) has looked at the effect of a shape resonance and the photoionization time delay. The present work on single-photon single ionization of the CO molecule by a single-laser XUV pulse without any dissociation differs from the previous studies [32–34] either in the number of pulses used or the ionization channel. Of note is that the laser-polarization-dependent PMD for the CO molecule computed semiclassically by a single laser pulse employed a wavelength of 532 nm, which requires a multiphoton absorption transition for single ionization [35]. The present work focuses on linear polarization of a single few-cycle XUV laser pulse, where the broad bandwidth nature of the ionizing laser pulse is such that more than one molecular orbital is likely to be ionized and the resulting energy spectra are thus expected to be mixed or entangled. Disentangling contributions of electrons emitted from different orbitals is a formidable task, which is extremely important for the correct analysis of the molecular imaging techniques including tomography imaging

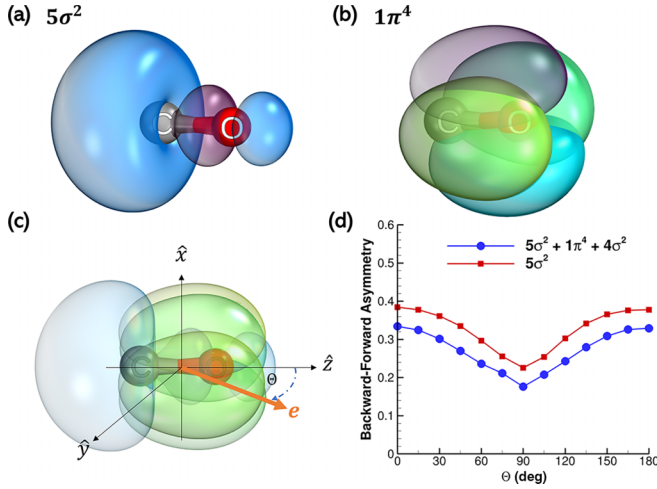


FIG. 1. (a) The asymmetric HOMO ( $5\sigma$ ) and (b) quasi-symmetric HOMO-1 ( $1\pi$ ) of the CO molecule. The threshold energies of the computed  $X^2\Sigma^+$  and  $A^2\Pi$  doublet states are 14.98 eV and 17.68 eV, in good agreement with the experimental data [46]. (c) The molecular orientation scheme used for our study, where  $\Theta$  is the angle between the molecular axis  $\mathbf{R}||\hat{z}$  and the polarization vector  $\mathbf{e}$ . (d) The variation of the normalized backward-forward asymmetry as a function of  $\Theta$ .

of molecular orbitals [36], laser-induced electron diffraction [37], time-resolved holography with photoelectrons [38], and multichannel photoemission in strong-field ionization [39]. However, Boguslavskiy *et al.* [39] addressed this issue for ionization of the two hydrocarbons *n*-butane and 1,3-butadiene. They found that ionization from inner orbitals is predominant in *n*-butane (minor in 1,3-butadiene) because of the small (large over 2 eV) energy gap between HOMO and HOMO-1 in these two molecules. A natural marker to achieve this goal was the absence of any fragmentation by HOMO ionization [39]. Switching the targets from these two hydrocarbons to the small CO molecule [with differently shaped outer and inner orbitals shown in Figs. 1(a) and 1(b) and separated by  $\sim 3$  eV] provides a unique possibility of exploring the backward-forward asymmetry as another natural marker to probe the degree of mixing between the HOMO and HOMO-1 ionization signal while the laser pulse electric field vector rotates in the polarization plane.

Our finding is threefold: (1) for the molecular axis  $\mathbf{R}$  aligned along the light polarization vector  $\mathbf{e}$ , the PMD exhibits a strong backward-forward asymmetry, which is unequivocally attributed to the asymmetric HOMO because of the smaller HOMO-1 signal contribution. (2) Rotating the laser polarization vector with respect to the molecular axis by an angle  $\Theta = (\mathbf{R}, \mathbf{e})$  in Fig. 1(c) allows us to manipulate the forward-backward asymmetry in the PMD while the changes in shape and magnitude controlled by the *m*-mixing problem [40] are explored and monitored. (3) When integrating the PMD over the photoelectron energy and polar angle in the forward and backward semicircles, the large normalized asymmetry from all contributing orbitals in Fig. 1(d) is weaker only by 5% compared to the dominant HOMO contribution for any molecular orientation, in concert with the findings in Ref. [39] for larger hydrocarbon molecules.

The organization of the present paper is as follows. In Sec. II, the details of the numerical laser experiment and the calculations are summarized. In Sec. III, the results for the PMD and their characteristic observations are given. Finally, Sec. IV presents the major findings and the conclusions.

## II. NUMERICAL METHODS

For the numerical experiment, we use a six-cycle sine-squared laser pulse linearly polarized (with an intensity of  $10^{12}$  W/cm<sup>2</sup> and a central carrier frequency  $\omega = 20$  eV corresponding to a duration  $T = 1.25$  fs) to study single-photon single ionization of the fundamental and closed-shell CO molecule with its moderate permanent electric dipole moment:

$$h\nu + \text{CO}(X^1\Sigma^+) \rightarrow \text{CO}^+(X^2\Sigma^+/A^2\Pi) + e^-(\mathbf{p}). \quad (1)$$

In contrast to the nonlinear ionization process in Ref. [39], the process (1) is linear in intensity. Because the pulse bandwidth  $\Delta\omega \approx 1.44\omega/n = 4.8$  eV (where  $n = 6$  cycles) is larger than the energy gap  $\Delta E \approx 3$  eV between the asymmetric HOMO and quasi symmetric HOMO-1 displayed in Figs. 1(a) and 1(b), this laser pulse interacts with these outer and inner orbitals of the ground electronic state ( $X^1\Sigma^+$ ) of the neutral molecule, and then creates entangled CEP-independent energy spectra for the continuum photoelectron with momentum  $\mathbf{p}$  while the molecular ion states for these two channels are the ground state  $X^2\Sigma^+$  or an excited state  $A^2\Pi$ .

The PMD for the single ionization of the closed-shell CO molecule is obtained by performing *ab initio* three-dimensional (3D) calculations. As the first step, the quantum chemical data of the CO molecule was obtained by running a MOLPRO [41] calculation with the restricted Hartree-Fock (RHF) method based on a correlation-consistent triple zeta basis. The ground electronic configuration of the molecule reads  $(1\sigma)^2(2\sigma)^2(3\sigma)^2(4\sigma)^2(1\pi)^4(5\sigma)^2$ . The frontier orbitals including the HOMO and the HOMO-1 are displayed in Figs. 1(a) and 1(b). In our present calculations, we have used a complete-active-space (CAS) description of the CO molecule where six electrons ( $1\sigma^2 2\sigma^2 3\sigma^2$ ) are frozen in the ground configuration. The remaining electrons are allowed to be in the active space of seven orbitals, including the three occupied  $4\sigma^2 1\pi^4 5\sigma^2$  orbitals and four unoccupied  $2\pi^0 6\sigma^0 7\sigma^0 3\pi^0$  orbitals. Ionizing an electron from  $5\sigma$  (HOMO) and  $1\pi$  (HOMO-1) orbitals leaves the  $\text{CO}^+$  ion in the doublet states  $X^2\Sigma^+$  and  $A^2\Pi$ , respectively. Next, to obtain the PMD of the ionized electron, we adopt the R-matrix method with the inclusion of time dependence (RMT). The details of the RMT method and its applications can be found elsewhere [42–45]. Briefly, the *ab initio* fixed-nuclei RMT method solves the time-dependent Schrödinger equation for multielectron atoms, ions, and molecules in laser fields within the electric dipole approximation. This is done by dividing the position space into inner and outer regions. The boundary of the inner and outer regions are marked by the R-matrix radius. The inner region accounts for the short-range electron-electron correlations, including exchange and Coulomb interactions, while the outer region contains the ionized electron, which interacts with the residual ion and the laser field. After propagating the outer-region wave function to a sufficiently large

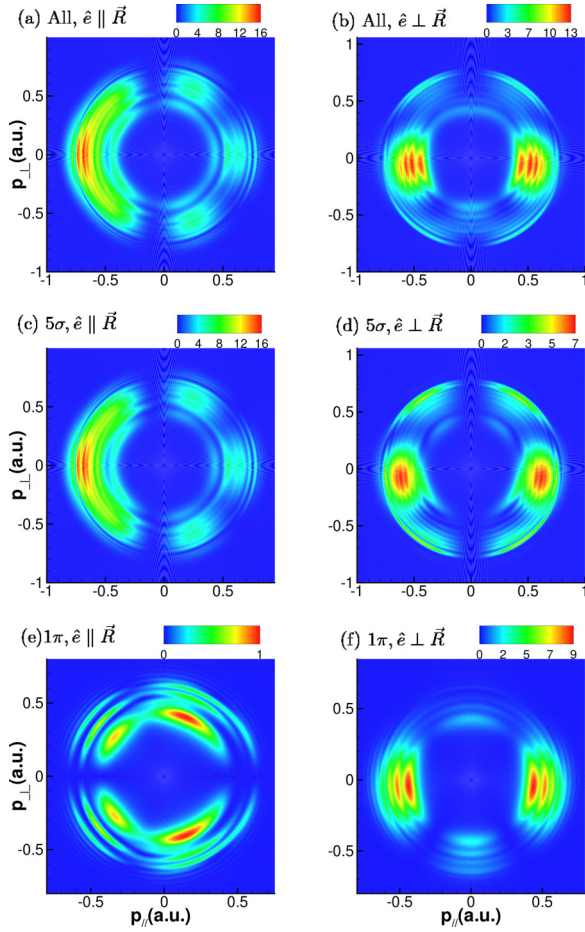


FIG. 2. The PMDs when the laser polarization vector  $\mathbf{e}$  is parallel [(a),(c),(e)] and perpendicular [(b),(d),(f)] to the molecular axis  $\mathbf{R}||\hat{z}$ , which is directed from the carbon atom to the oxygen atom. The laser is propagating along the  $x$  axis and the polarization vector lies on the  $yz$  plane. In both cases, the contributions from all occupied orbitals in the active space are shown in (a) and (b). The individual contributions to the PMD from HOMO [(c),(d)] and HOMO-1 [(e),(f)] are also shown.

distance ( $\sim 4000$  a.u.), a Fourier transform is applied to the radial wave function to obtain the PMD.

### III. NUMERICAL RESULTS

Figure 2(a) shows the PMD obtained in the parallel configuration ( $\Theta = 0$ ), i.e., when the fixed-in-space CO is oriented along the light's polarization vector  $\mathbf{e}$ . For the present RMT calculations, we have included three target states corresponding to ionizing an electron from  $5\sigma$  (HOMO),  $1\pi$  (HOMO-1), and  $4\sigma$  (HOMO-2) orbitals. As the main finding, one sees that the PMD in Fig. 2(a) exhibits a strong backward-forward asymmetry, which is the HOMO fingerprint, explained as follows. For the present photon energy with its bandwidth, it is possible that the HOMO-2 (21.92 eV) also contributes to the ionization. However, the extremely small ionization signal from HOMO-2 is significantly shadowed by the HOMO and it is hardly visible in the overall PMD. Therefore, the individual contributions to the PMD from HOMO and HOMO-1 are shown in Figs. 2(c) and 2(e), respectively. Remarkably,

the shapes of the electronic density in HOMO and HOMO-1 displayed in Figs. 1(a) and 1(b) are quite well reflected in the PMDs in Figs. 2(c) and 2(e). However, as the HOMO-1 signal is one order of magnitude smaller than the HOMO signal, their mixing gives an asymmetric pattern [Fig. 2(a)] that coincides essentially with the HOMO contribution shown in Fig. 2(c).

But where does the asymmetry feature come from in the HOMO of CO and how does it build up in the continuum? First, the oxygen atom in CO is more electronegative than the carbon atom. Thus, the atomic  $2s$  and  $2p$  orbitals of O have lower energies than that of C. Consequently, as the two atoms bond, there is a favorable interaction between the oxygen's  $2p_z$  (-15.85 eV) orbital and both carbon's  $2s$  (-19.43 eV) and  $2p_z$  (-10.66 eV) orbitals [47]. According to the energy difference, the contribution from carbon's  $2s$  orbital to the bonding HOMO dominates (see, e.g., the Hartree-Fock-Roothaan calculations for CO given in Table AB-41 of Ref. [48]). This will then substantially deform the distribution of HOMO, shifting it more toward the carbon atom, see Fig. 1(a).

The initial HOMO is expressed as a linear combination of atomic  $s$ ,  $p$ ,  $d$ -type orbitals which are centered at the atom locations. For our discussion of the selection rules, the angular component of the initial orbital can be thought of as an expansion in a complete basis of the spherical harmonics which are centered at the origin (center of mass). The partial waves describing the continuum unbound electron can be deduced according to the electric dipole selection rules and the symmetry considerations discussed in the Appendix. The one-photon transitions from different angular components of the HOMO to the continuum occur according to electric dipole selection rules to yield the PMD. In the following, we show this by analyzing the partial contributions to the PMD from each of these channels in which the ionized electron is coupled to the residual ion. In the RMT approach, the final PMD is obtained by [43]

$$\mathcal{W}(\mathbf{p}) = \sum_i \left| \sum_{\Gamma, lm} \tilde{F}_{i,lm}^{\Gamma}(|\mathbf{p}|) X_{lm}(\hat{\mathbf{p}}) \right|^2, \quad (2)$$

where the summation  $i$  runs over all residual-ion states and  $\Gamma$  runs over the irreducible representations of the point group of the molecule [49], see Appendix. Here, only three nondissociative states,  $X^2\Sigma^+$ ,  $A^2\Pi$ , and  $B^2\Sigma^+$ , of the ion  $\text{CO}^+$  are included in our numerical calculations, which are associated respectively with the ionization from HOMO, HOMO-1, and HOMO-2. Here,  $l, m$  correspond to the electron continuum angular momentum and its  $z$  projection in each channel such that when the symmetry of the real spherical harmonic  $X_{l,m}(\hat{\mathbf{p}})$  is combined with the symmetry of the residual-ion state, the overall symmetry of the molecule is recovered. The coefficient  $\tilde{F}_{i,lm}^{\Gamma}(|\mathbf{p}|)$  is the Fourier transform of the reduced radial wave function in the outer region [42–45]. For the parallel configuration where only HOMO is allowed in the active space, we show in Fig. 3 the partial contributions from the  $(l, m) = (1, 0)$ ,  $(2, 0)$ , and  $(3, 0)$  channels to see how the PMD in Fig. 2(c) builds up. Although other values of  $(l, m)$  do contribute to the total PMD according to their symmetries, the  $(1, 0)$ ,  $(2, 0)$ , and  $(3, 0)$  channels have the most significant contributions. In Figs. 3(a)–3(c), the individual contributions from the  $l = 1, 2, 3$  channels (with  $m = 0$ ) are then shown.

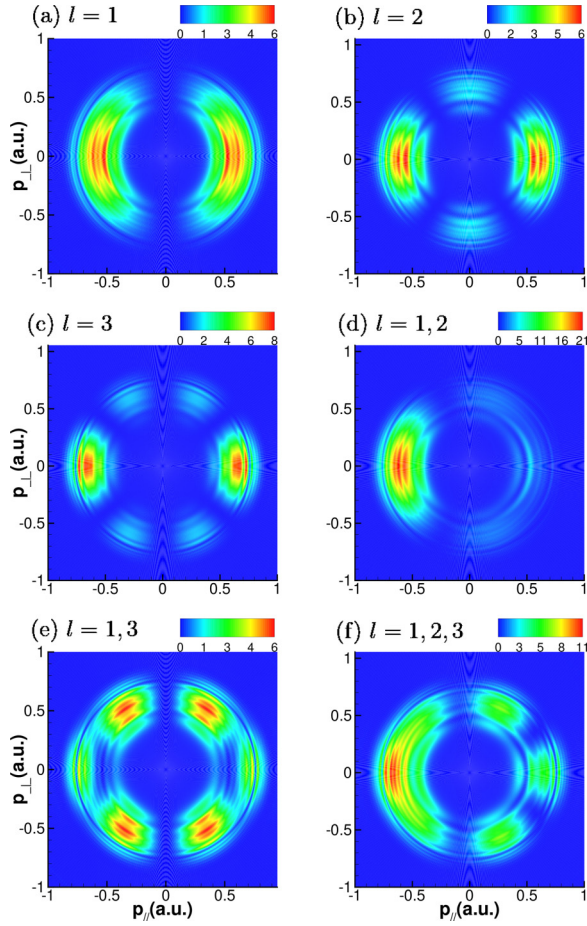


FIG. 3. Buildup of the forward-backward asymmetry in the PMD in Fig. 2(c) from the HOMO when the molecular axis  $\mathbf{R}||\hat{\mathbf{z}}$  is parallel to the laser polarization vector  $\mathbf{e}$ . The computed partial contributions to the PMD are shown for (a)  $l = 1$ , (b)  $l = 2$ , and (c)  $l = 3$ . Here,  $l$  is the angular momentum of the continuum electron. The isotropic ring-like partial contribution from  $l = 0$  (not shown) is at least an order of magnitude smaller. Shown in (d), (e), and (f) are the mixture between the partial contributions from  $l = 1, 2, l = 1, 3$ , and  $l = 1, 2, 3$ , respectively. Note that  $m = 0$  for all  $l$  values above because the laser pulse is linearly polarized.

For example, the dipole-like PMD in Fig. 3(a) for the  $l = 1$  channel has a symmetry character of a  $p^0$  partial wave. Similarly, when  $l = 2$  and  $l = 3$ , the twofold quadrupole-like and hexapole-like PMDs in Figs. 3(b) and 3(c) resemble the symmetries of  $d^0$  and  $f^0$  partial waves, respectively. According to electric dipole selection rules, the bound-to-continuum one-photon transitions  $s \rightarrow p^0$  and  $d^0 \rightarrow p^0$  produce the partial PMD in Fig. 3(a). Likewise, the partial PMDs in Figs. 3(b) and 3(c) are obtained by the one-photon transition  $p^0 \rightarrow d^0$  and  $d^0 \rightarrow f^0$ , respectively. When the amplitudes for the partial PMDs for  $p^0$  and  $d^0$  with comparable magnitudes are coherently mixed, because of their opposite parity the resulting interference pattern displayed in Fig. 3(d) exhibits a strong asymmetric character toward the carbon side. In contrast, mixing the amplitudes for the partial PMDs for  $p^0$  and  $f^0$  with the same parity and comparable magnitudes does not lead to an asymmetric interferogram, but instead to a symmetric interferogram, shown in Fig. 3(e). Finally, adding coherently

the  $f^0$  amplitude to the  $p^0 + d^0$  amplitude in Fig. 3(d) leads to the asymmetric interferogram shown in Fig. 3(f). It is important that the transition  $p^0 \rightarrow s$  is allowed, but this isotropic ring-like partial contribution (not shown) is at least an order of magnitude smaller than the other partial contributions. The little difference between the patterns in Fig. 3(f) and Fig. 2(c) supports our claim. It also shows that the three ionization side peaks or satellite peaks (located at  $\theta = \pi/3, 0, -\pi/3$ ) seen in the forward direction in Fig. 2(c) stem from mixing the  $d^0$  and  $f^0$  amplitudes with identical parity, whereas the main peak in the backward direction originates from mixing the  $p^0$  and  $d^0$  amplitudes with opposite parity. All these demonstrate that the backward-forward asymmetry in the PMD [Fig. 2(c)] is due to the interference among the  $p^0$ ,  $d^0$ , and  $f^0$  ionization channels in HOMO.

For the antiparallel scheme ( $\Theta = \pi$ ), the asymmetry in the PMD flips and now peaks toward the oxygen side as expected, see our RMT results in the Supplemental Material [50]. Given the  $m$ -mixing problem [40] known to dramatically transform the shape of the PMDs as  $\mathbf{e}$  rotates, a natural question then arises on whether the molecular orientation with respect to the light polarization vector affects the asymmetry in the PMD. Our results in Fig. 2(b) for the PMD when including all the contributions (HOMO, HOMO-1, HOMO-2) in the active space show that the backward-forward asymmetry, stronger for the parallel configuration [Fig. 2(a)] at  $\theta = \Theta = 0$ , disappears completely for the perpendicular configuration [Fig. 2(b)] at  $\theta = \Theta = \pi/2$ . Moreover, in Fig. 2(b) the patterns on the left and right sides with respect to light polarization vector axis are symmetric, whereas the patterns on the upper and lower semicircles with respect to the molecular axis are not. The individual contributions to the PMD from HOMO and HOMO-1 are shown in Figs. 2(d) and 2(f), respectively. For this perpendicular configuration, we can see that the contribution from HOMO-1 is larger than that from HOMO. However, the contribution from HOMO is still significant, leading to a stronger degree of mixing for  $\Theta = \pi/2$  than for  $\Theta = 0$ . Because the final states of the system electron with momentum  $\mathbf{p} + \text{photoion}$  are different, the implication is that the contributions to the PMD from the two molecular orbitals add up incoherently when  $\Theta = \pi/2$ .

For other molecular orientations, Ref. [50] shows a movie for the evolution of the PMD as  $\Theta$  changes from 0 to  $2\pi$  with small step corresponding to 26 snapshots, which can be realized using impulsive alignment to control the angle  $\Theta$  [51,52]. The great sensitivity of the shape of the PMD to the orientation angle  $\Theta$  is clearly observed, which is due to the  $m$ -mixing problem [40]. When  $\Theta$  varies from 0 to  $\pi$ , the angles for which the backward-forward asymmetry ceases to be a good marker for the observable PMD because of the  $m$ -mixing problem [40] are  $\Theta \in [\pi/6, 5\pi/6]$ . However, an observable transparent to the  $m$ -mixing problem which provides a rough estimate on the degree of mixed spectra is the variation of the normalized asymmetry  $A \equiv (\mathcal{W}_- - \mathcal{W}_+)/(\mathcal{W}_- + \mathcal{W}_+)$  as a function of  $\Theta$ , where  $\mathcal{W}_+$  and  $\mathcal{W}_-$  refer to the energy- and angular-integrated PMDs in the forward and backward semicircles obtained at a fixed  $\Theta$ . Figure 1(d) shows that the normalized asymmetry either from the HOMO or from all contributing orbitals is very large, ranging from 18% to 38%, which is comparable to what has been predicted for the

correlated nonlinear process of single ionization of helium where the residual ion remains in the  $n = 2$  states [10]. Interestingly, the normalized asymmetry in Fig. 1(d) from HOMO exceeds that from all contributions (HOMO, HOMO-1, HOMO-2) by roughly 5%–6% regardless of the molecular orientation, confirming the results seen in larger hydrocarbon molecules [39] that ionization from the outer orbital dominates over that from the inner orbital when their energy gap is over 2 eV.

#### IV. SUMMARY AND CONCLUSIONS

In summary, we have deployed the *ab initio* RMT method to investigate the backward-forward asymmetry through photoionization of the CO molecule by a linearly polarized XUV pulse. Because of the broad pulse bandwidth, electrons are pulled out from the HOMO and HOMO-1, thus leading to a mixed PMD. However, although there is no interference between these two ionization channels because the final states of the molecular ion are different, there are strong interferences within each ionization channel. We used the backward-forward asymmetry (inherent to the HOMO) in the PMD and normalized asymmetry as probes of the degree of mixed spectra, and found that the HOMO contribution is dominant for any molecular orientation. Our investigations for the molecular backward-forward asymmetry illustrated here for the CO molecule (for which the permanent electric dipole moment is moderate) can be extended to other molecules (e.g., HF) with larger permanent electric dipole moment.

#### ACKNOWLEDGMENTS

This work is supported by the US Department of Energy (DOE), Office of Science, Basic Energy Sciences (BES), under Award No. DE-SC0021054. This work was completed utilizing Swan of the Holland Computing Center of the University of Nebraska, which receives support from the Nebraska Research Initiative.

#### APPENDIX: SYMMETRY CONSIDERATIONS

The properties of the PMDs discussed above can be explained by the symmetry arguments. The process of single-photon ionization in the electric dipole approximation can be explained by the probability amplitude within the fixed-nuclei approximation ( $R = 1.128$  a.u.),

$$\mathcal{A}(\mathbf{p}) = \langle \psi^{N-1}(\chi_{N-1})\phi_{\mathbf{p}}^e(\mathbf{r}) | \mu | \psi^N(\chi_N) \rangle, \quad (\text{A1})$$

where  $\chi_N \equiv (\mathbf{r}_1, \mathbf{r}_2, \dots, \mathbf{r}_N; \mathbf{R})$ ,  $\mathbf{r} \equiv \mathbf{r}_N$ , and  $N$  is the total number of electrons in the neutral molecule. Here,  $\mu$  is the electric dipole operator, and  $\psi^N(\chi_N)$  and  $\psi^{N-1}(\chi_{N-1})\phi_{\mathbf{p}}^e(\mathbf{r})$  are the single-determinant Hartree-Fock wave functions of the initial and final states, respectively. The photoelectron is described by the wave function  $\phi_{\mathbf{p}}^e(\mathbf{r})$ , where  $\mathbf{p}$  is its momentum. We do not consider spin effects, therefore for simplicity the spin variables are omitted. Note that all the quantities appearing in Eq. (A1) are expressed in the molecular frame. Often, the photoelectron wave function is expanded using

partial waves,

$$\phi_{\mathbf{p}}^e(\mathbf{r}) = \sqrt{\frac{2}{\pi}} \sum_{lm} i^l e^{-i\eta_l(p)} Y_{l,m}^*(\hat{\mathbf{p}}) Y_{l,m}(\hat{\mathbf{r}}) R_{p,l}(r), \quad (\text{A2})$$

where  $\eta_l(p)$  accounts for the partial wave phase shifts due to Coulomb, exchange, and short-range interaction between the photoelectron and the ionized molecule. Once this expansion (A2) is substituted into Eq. (A1), the remaining radial integration can be simplified in terms of symmetry arguments. If we use the irreducible representations  $\Gamma(\psi^N)$ ,  $\Gamma(\psi^{N-1})$ ,  $\Gamma(\phi_{\mathbf{p}}^e)$ , and  $\Gamma(\mu)$  to characterize the symmetries of the neutral state, ionic state, photoelectron, and the electric dipole operator, respectively, then the probability amplitude  $\mathcal{A}$  in Eq. (A1) is nonvanishing only if the direct product  $\Gamma(\psi^{N-1}) \otimes \Gamma(\phi_{\mathbf{p}}^e) \otimes \Gamma(\mu) \otimes \Gamma(\psi^N)$  contains the totally symmetric representation  $\Gamma^s$  of the symmetry group [53], i.e.,

$$\Gamma(\psi^{N-1}) \otimes \Gamma(\phi_{\mathbf{p}}^e) \otimes \Gamma(\mu) \otimes \Gamma(\psi^N) \supset \Gamma^s. \quad (\text{A3})$$

In the RMT code, the  $C_{2v}$  point group is used to describe the symmetry of the CO molecule instead of the  $C_{\infty v}$  point group to which the actual symmetry of CO belongs. Therefore, in the terminology of the  $C_{2v}$  group's irreducible representations [53] and taking the molecular axis as the symmetry axis,  $\Gamma(\psi^N) = a_1$  for closed-shell neutral molecules with  $C_{2v}$  symmetry, and  $\Gamma(\psi^{N-1}) = a_1$  if ionized from HOMO or  $\Gamma(\psi^{N-1}) = b_1, b_2$  if ionized from HOMO-1. When the polarization is parallel to the molecular axis (i.e., when the laboratory frame's  $z$  axis coincides with the molecular frame's  $z$  axis, which is also the symmetry axis), then the irreducible representation of the electric dipole operator becomes  $\Gamma(\mu_z) = a_1$ . Hence, it is readily seen from Eq. (A3) that  $\Gamma(\phi_{\mathbf{p}}^e) = a_1$  if the ionization occurs from HOMO. This corresponds to the partial waves ( $l, m$ ) of the ejected electron with  $a_1$  symmetry such as (0, 0), (1, 0), (2, 0), and (3, 0) (as shown in Fig. 3). Note that even if some partial waves are allowed according to their irreducible representation in the  $C_{2v}$  group, these partial waves still have to satisfy the dipole selection rules. The dipole- and symmetry-allowed partial waves then interfere constructively or destructively (according to their parities), producing the observed PMDs. The higher partial waves  $l > 1$  are possible if the angular components of the initial wave function  $\psi^N$  contains spherical harmonics with  $l \geq 1$ . And if the ionization occurs from HOMO-1 for the same parallel configuration, then the partial waves for the electron should possess either  $\Gamma(\phi_{\mathbf{p}}^e) = b_1$  or  $\Gamma(\phi_{\mathbf{p}}^e) = b_2$  symmetry. Now, when the polarization vector  $\mathbf{e}$  is perpendicular to the molecular axis, (in other words, the vector  $\mathbf{e}$  is parallel to the molecular frame's  $x$  or  $y$  axis), then, in the perspective of the molecular frame,  $\Gamma(\mu_x) = b_1$  or  $\Gamma(\mu_y) = b_2$ . Therefore, if the ionization occurs from HOMO and according to Eq. (A3), we expect the partial waves of the electron to have either  $\Gamma(\phi_{\mathbf{p}}^e) = b_1$  or  $\Gamma(\phi_{\mathbf{p}}^e) = b_2$  symmetry. If the ionization occurs from HOMO-1 for the perpendicular configuration, then it is again clear that the partial waves of the electron have  $\Gamma(\phi_{\mathbf{p}}^e) = a_1$  symmetry.

- [1] F. Krausz and M. Ivanov, *Rev. Mod. Phys.* **81**, 163 (2009).
- [2] M. Nisoli, P. Declève, F. Calegari, A. Palacios, and F. Martín, *Chem. Rev.* **117**, 10760 (2017).
- [3] E. Cormier and P. Lambropoulos, *Eur. Phys. J. D* **2**, 15 (1998).
- [4] A. Gürtler, F. Robicheaux, W. J. van der Zande, and L. D. Noordam, *Phys. Rev. Lett.* **92**, 033002 (2004).
- [5] V. Roudnev and B. D. Esry, *Phys. Rev. Lett.* **99**, 220406 (2007).
- [6] L.-Y. Peng, E. A. Pronin, and A. F. Starace, *New J. Phys.* **10**, 025030 (2008).
- [7] E. A. Pronin, A. F. Starace, M. V. Frolov, and N. L. Manakov, *Phys. Rev. A* **80**, 063403 (2009).
- [8] E. A. Pronin, A. F. Starace, and L.-Y. Peng, *Phys. Rev. A* **84**, 013417 (2011).
- [9] J. M. N. Djiokap, S. X. Hu, W.-C. Jiang, L.-Y. Peng, and A. F. Starace, *New J. Phys.* **14**, 095010 (2012).
- [10] J. M. N. Djiokap, S. X. Hu, W.-C. Jiang, L.-Y. Peng, and A. F. Starace, *Phys. Rev. A* **88**, 011401(R) (2013).
- [11] J. M. Ngoko Djiokap, N. L. Manakov, A. V. Meremianin, and A. F. Starace, *Phys. Rev. A* **88**, 053411 (2013).
- [12] M. Hentschel, R. Kienberger, C. Spielmann, G. A. Reider, N. Milosevic, T. Brabec, P. Corkum, U. Heinzmann, M. Drescher, and F. Krausz, *Nature (London)* **414**, 509 (2001).
- [13] R. Kienberger, E. Goulielmakis, M. Uiberacker, A. Baltuska, V. Yakovlev, F. Bammer, A. Scrinzi, T. Westerwalbesloh, U. Kleineberg, U. Heinzmann, M. Drescher, and F. Krausz, *Nature (London)* **427**, 817 (2004).
- [14] G. Sansone, E. Benedetti, F. Calegari, C. Vozzi, L. Avaldi, R. Flammini, L. Poletto, P. Villoresi, C. Altucci, R. Velotta, S. Stagira, S. De Silvestri, and M. Nisoli, *Science* **314**, 443 (2006).
- [15] E. Goulielmakis, M. Schultze, M. Hofstetter, V. S. Yakovlev, J. Gagnon, M. Uiberacker, A. L. Aquila, E. M. Gullikson, D. T. Attwood, R. Kienberger, F. Krausz, and U. Kleineberg, *Science* **320**, 1614 (2008).
- [16] S. Gilbertson, Y. Wu, S. D. Khan, M. Chini, K. Zhao, X. Feng, and Z. Chang, *Phys. Rev. A* **81**, 043810 (2010).
- [17] K. Zhao, Q. Zhang, M. Chini, Y. Wu, X. Wang, and Z. Chang, *Opt. Lett.* **37**, 3891 (2012).
- [18] P.-C. Huang, C. Hernández-García, J.-T. Huang, P.-Y. Huang, C.-H. Lu, L. Rego, D. D. Hickstein, J. L. Ellis, A. Jaron-Becker, A. Becker, S.-D. Yang, C. G. Durfee, L. Plaja, H. C. Kapteyn, M. M. Murnane, A. H. Kung, and M.-C. Chen, *Nat. Photonics* **12**, 349 (2018).
- [19] P. Agostini, F. Fabre, G. Mainfray, G. Petite, and N. K. Rahman, *Phys. Rev. Lett.* **42**, 1127 (1979).
- [20] E. J. Takahashi, P. Lan, O. D. Mücke, Y. Nabekawa, and K. Midorikawa, *Phys. Rev. Lett.* **104**, 233901 (2010).
- [21] F. Ferrari, F. Calegari, M. Lucchini, C. Vozzi, S. Stagira, G. Sansone, and M. Nisoli, *Nat. Photonics* **4**, 875 (2010).
- [22] T. Popmintchev, M.-C. Chen, P. Arpin, M. M. Murnane, and H. C. Kapteyn, *Nat. Photonics* **4**, 822 (2010).
- [23] P. Tzallas, E. Skantzakis, L. A. A. Nikolopoulos, G. D. Tsakiris, and D. Charalambidis, *Nat. Phys.* **7**, 781 (2011).
- [24] J. Duris, S. Li, T. Driver, E. G. Champenois, J. P. MacArthur, A. A. Lutman, Z. Zhang, P. Rosenberger, J. W. Aldrich, R. Coffee, G. Coslovich, F.-J. Decker, J. M. Glowina, G. Hartmann, W. Helml, A. Kamalov, J. Knurr, J. Krzywinski, M.-F. Lin, J. P. Marangos *et al.*, *Nat. Photonics* **14**, 30 (2020).
- [25] P. K. Maroju, C. Grazioli, M. Di Fraia, M. Moio, D. Ertel, H. Ahmadi, O. Plekan, P. Finetti, E. Allaria, L. Giannessi, G. De Ninno, C. Spezzani, G. Penco, S. Spampinati, A. Demidovich, M. B. Danailov, R. Borghes, G. Kourousias, C. E. Sanches Dos Reis, F. Billé *et al.*, *Nature (London)* **578**, 386 (2020).
- [26] S. Nandi, E. Olofsson, M. Bertolino, S. Carlström, F. Zapata, D. Busto, C. Callegari, M. Di Fraia, P. Eng-Johnsson, R. Feifel, G. Gallician, M. Gisselbrecht, S. Maclot, L. Neoričić, J. Peschel, O. Plekan, K. C. Prince, R. J. Squibb, S. Zhong, P. V. Demekhin *et al.*, *Nature (London)* **608**, 488 (2022).
- [27] P. K. Maroju, M. Di Fraia, O. Plekan, M. Bonanomi, B. Merzuk, D. Busto, I. Makos, M. Schmoll, R. Shah, P. R. Ribič, L. Giannessi, G. De Ninno, C. Spezzani, G. Penco, A. Demidovich, M. Danailov, M. Coreno, M. Zangrando, A. Simoncig, M. Manfredda *et al.*, *Nat. Photonics* **17**, 200 (2023).
- [28] G. Perosa, J. Wätzel, D. Garzella, E. Allaria, M. Bonanomi, M. B. Danailov, A. Brynes, C. Callegari, G. De Ninno, A. Demidovich, M. Di Fraia, S. Di Mitri, L. Giannessi, M. Manfredda, L. Novinec, N. Pal, G. Penco, O. Plekan, K. C. Prince, A. Simoncig *et al.*, *Phys. Rev. Lett.* **131**, 045001 (2023).
- [29] K. C. Prince, E. Allaria, C. Callegari, R. Cucini, G. De Ninno, S. Di Mitri, B. Diviacco, E. Ferrari, P. Finetti, D. Gauthier, L. Giannessi, N. Mahne, G. Penco, O. Plekan, L. Raimondi, P. Rebernik, E. Roussel, C. Svetina, M. Trovò, M. Zangrando *et al.*, *Nat. Photonics* **10**, 176 (2016).
- [30] G. Laurent, W. Cao, H. Li, Z. Wang, I. Ben-Itzhak, and C. L. Cocke, *Phys. Rev. Lett.* **109**, 083001 (2012).
- [31] J. Fuchs, N. Douguet, S. Donsa, F. Martín, J. Burgdörfer, L. Argenti, L. Cattaneo, and U. Keller, *Phys. Rev. Res.* **3**, 013195 (2021).
- [32] A. Chacón and C. Ruiz, *Opt. Express* **26**, 4548 (2018).
- [33] J. Vos, L. Cattaneo, S. Patchkovskii, T. Zimmermann, C. Cirelli, M. Lucchini, A. Kheifets, A. S. Landsman, and U. Keller, *Science* **360**, 1326 (2018).
- [34] X. Gong, W. Jiang, J. Tong, J. Qiang, P. Lu, H. Ni, R. Lucchese, K. Ueda, and J. Wu, *Phys. Rev. X* **12**, 011002 (2022).
- [35] X. Zhu, Q. Zhang, W. Hong, P. Lu, and Z. Xu, *Opt. Express* **19**, 24198 (2011).
- [36] J. Itatani, J. Levesque, D. Zeidler, H. Niikura, H. Pépin, J. C. Kieffer, P. B. Corkum, and D. M. Villeneuve, *Nature (London)* **432**, 867 (2004).
- [37] T. Zuo, A. D. Bandrauk, and P. B. Corkum, *Chem. Phys. Lett.* **259**, 313 (1996).
- [38] Y. Huismans, A. Rouzée, A. Gijsbertsen, J. H. Jungmann, A. S. Smolkowska, P. S. W. M. Logman, F. Lépine, C. Cauchy, S. Zamith, T. Marchenko, J. M. Bakker, G. Berden, B. Redlich, A. F. G. van der Meer, H. G. Muller, W. Vermin, K. J. Schafer, M. Spanner, M. Y. Ivanov, O. Smirnova *et al.*, *Science* **331**, 61 (2011).
- [39] A. E. Boguslavskiy, J. Mikosch, A. Gijsbertsen, M. Spanner, S. Patchkovskii, N. Gador, M. J. J. Vrakking, and A. Stolow, *Science* **335**, 1336 (2012).
- [40] T. K. Kjeldsen, L. A. A. Nikolopoulos, and L. B. Madsen, *Phys. Rev. A* **75**, 063427 (2007).
- [41] H.-J. Werner, P. J. Knowles, G. Knizia, F. R. Manby, and M. Schütz, *WIREs Comput. Mol. Sci.* **2**, 242 (2012).
- [42] L. Moore, M. Lysaght, L. Nikolopoulos, J. Parker, H. van der Hart, and K. Taylor, *J. Mod. Opt.* **58**, 1132 (2011).
- [43] A. C. Brown, G. S. Armstrong, J. Benda, D. D. Clarke, J. Wragg, K. R. Hamilton, Z. Mašín, J. D. Gorfinkiel, and H. W. van der Hart, *Comput. Phys. Commun.* **250**, 107062 (2020).

- [44] M. A. Lysaght, H. W. van der Hart, and P. G. Burke, *Phys. Rev. A* **79**, 053411 (2009).
- [45] D. D. A. Clarke, G. S. J. Armstrong, A. C. Brown, and H. W. van der Hart, *Phys. Rev. A* **98**, 053442 (2018).
- [46] M. Yousif, D. E. Ramaker, and H. Sambe, *Chem. Phys. Lett.* **101**, 472 (1983).
- [47] J. B. Mann, T. L. Meek, and L. C. Allen, *J. Am. Chem. Soc.* **122**, 2780 (2000).
- [48] P. E. Cade and W. M. Huo, *At. Data Nucl. Data Tables* **15**, 1 (1975).
- [49] N. Chandra, *J. Phys. B* **20**, 3405 (1987).
- [50] See Supplemental Material at <http://link.aps.org/supplemental/10.1103/PhysRevA.109.043108> for an evolution of the PMD as  $\Theta$  changes from 0 to  $2\pi$  with small steps corresponding to 26 snapshots, NA 00, 000 (0000).
- [51] T. Seideman, *Phys. Rev. Lett.* **83**, 4971 (1999).
- [52] F. Rosca-Pruna and M. J. J. Vrakking, *Phys. Rev. Lett.* **87**, 153902 (2001).
- [53] P. R. Bunker and P. Jensen, *Molecular Symmetry and Spectroscopy*, 2nd ed. (NRC Research Press, Ottawa, 1998).